Title

The PSI—PSII Megacomplex in Green Plants

Journal

Plant and Cell Physiology, 60(5)

ISSN

0032-0781

Authors

Yokono, Makio

Takabayashi, Atsushi

Kishimoto, Junko

et al.

Publication Date

2019-05-01

DOI

10.1093/pcp/pcz026

Peer reviewed

PCP
PLANT & CELL PHYSIOLOGY

The PSI–PSII Megacomplex in Green Plants

Makio Yokono[1,2,3,*], Atsushi Takabayashi[1,2], Junko Kishimoto[1,2], Tomomichi Fujita[4], Masakazu Iwai[5,6], Akio Murakami[7,8], Seiji Akimoto[8] and Ayumi Tanaka[1,2]

[1]Institute of Low Temperature Science, Hokkaido University, Sapporo 060–0819, Japan
[2]CREST, JST, Sapporo 060–0819, Japan
[3]Nippon Flour Mills Co., Ltd., Innovation Center, Atsugi 243–0041, Japan
[4]Department of Biological Sciences, Faculty of Science, Hokkaido University, Sapporo 060–0810, Japan
[5]Department of Plant and Microbial Biology, University of California, Berkeley, CA 94720–3102, USA
[6]Molecular Biophysics and Integrated Bioimaging Division, Lawrence Berkeley National Laboratory, Berkeley, CA 94720, USA
[7]Kobe University Research Centre for Inland Seas, Awaji 656–2401, Japan
[8]Graduate School of Science, Kobe University, Kobe 657–8501, Japan
*Corresponding author: E-mail, filia@mac.com; Fax, +81-11-706-5493.
(Received May 23, 2018; Accepted February 4, 2019)

Energy dissipation is crucial for land and shallow-water plants exposed to direct sunlight. Almost all green plants dissipate excess excitation energy to protect the photosystem reaction centers, photosystem II (PSII) and photosystem I (PSI), and continue to grow under strong light. In our previous work, we reported that about half of the photosystem reaction centers form a PSI–PSII megacomplex in *Arabidopsis thaliana*, and that the excess energy was transferred from PSII to PSI fast. However, the physiological function and structure of the megacomplex remained unclear. Here, we suggest that high-light adaptable sun-plants accumulate the PSI–PSII megacomplex more than shade-plants. In addition, PSI of sun-plants has a deep trap to receive excitation energy, which is low-energy chlorophylls showing fluorescence maxima longer than 730 nm. This deep trap may increase the high-light tolerance of PSI by improving excitation energy dissipation. Electron micrographs suggest that one PSII dimer is directly sandwiched between two PSIs with 2-fold rotational symmetry in the basic form of the PSI–PSII megacomplex in green plants. This structure should enable fast energy transfer from PSII to PSI and allow energy in PSII to be dissipated via the deep trap in PSI.

Keywords: Energy transfer • Nonphotochemical quenching • Photosystem.

Introduction

Photosynthetic organisms perform efficient photosynthesis under fluctuating environmental conditions. To achieve this, the photosystems must supply electrons to meet the needs of ferredoxin-dependent processes such as carbon dioxide fixation and nitrogen assimilation. Furthermore, the generation of reactive oxygen species by excited photosystems must also be suppressed. To satisfy these requirements, photosynthetic organisms have developed various regulatory mechanisms such as antenna size regulation (Masuda et al. 2003), state transition (Rochaix 2007), nonphotochemical quenching (Ruban 2016) and spillover (Chow et al. 1981).

Spillover is considered a mechanism to balance excitation between the two types of photosystem reaction centers, photosystem I (PSI) and photosystem II (PSII). Satoh et al. (1976) found that energy transfer from PSII to PSI greatly increased when the PSII reaction centers were closed in spinach chloroplasts. Tan et al. (1998) proposed that PSI migrates toward the central region of the grana stack and associates with PSII in the state transition, which enhances spillover from PSII to PSI. Theoretically, spillover requires a tight interaction between PSI and PSII because excitation energy transfer does not occur between distantly located pigments. Järvi et al. (2011) isolated a PSI–PSII megacomplex using large-pore blue-native polyacrylamide gel electrophoresis, which can separate large and unstable complexes. We also isolated PSI–PSII megacomplexes from digitonin-solubilized thylakoid membranes by large-pore clear-native polyacrylamide gel electrophoresis (lpCN-PAGE; Yokono et al. 2015). Time-resolved fluorescence analysis of the PSI–PSII megacomplexes isolated by lpCN-PAGE showed that excitation energy produced by charge recombination in PSII was transferred to PSI and emitted as fluorescence (Yokono et al. 2015). This provided direct evidence that spillover occurs in the PSI–PSII megacomplex. Cyanobacteria also have megacomplexes composed of PSI, PSII and phycobilisomes, but no energy transfer between PSI and PSII was observed in isolated megacomplexes (Liu et al. 2013).

Many reports have indicated that most PSII and PSI reaction centers exist in the grana core and stromal thylakoids, respectively, in chloroplasts (Anderson 2012). If PSI and PSII are located separately in different membrane regions, they would have no chance to form a megacomplex. Fractionation experiments on thylakoid membranes indicate that only 16–18% of the chlorophyll is located in stroma lamellae (Albertsson 2001) and the remaining chlorophyll is located in grana including the grana core and grana margin. The exact distribution of PSI and PSII among these membrane regions has not been elucidated yet and contradictory results have been reported concerning the composition of PSI and PSII in the grana margin, which contains 30–40% of the total chlorophyll (Andersson and Anderson

Plant Cell Physiol. 0(0): 1–11 doi:10.1093/pcp/pcz026, Advance Access publication on 11 February 2019, available online at https://academic.oup.com/pcp

1980). One report showed that PSII was not located in the grana margin (Albertsson 2001), but another report showed that the PSI/PSII ratio in the grana margin was 1.28 (Veerman et al. 2007). If the grana margin contains both PSI and PSII, PSI–PSII megacomplexes could exist there. Järvi et al. (2011) and our research group both reported that PSI–PSII megacomplexes exist in digitonin-solubilized thylakoid membranes, which contain grana margins and stromal thylakoids (Yokono et al. 2015), suggesting that a PSI–PSII megacomplex exists in the grana margin. The membrane structures of chloroplasts are similar among vascular plants, in which grana stacks are well developed and the relative amount of stromal lamellae is constant (Albertsson 2001). In contrast, green alga *Chlamydomonas* thylakoid membranes are loosely arranged with more free-floating stroma lamellae interrupted by a few pseudograna structures (Mussgnug et al. 2005). In green alga *Ostreococcus*, the grana are composed of three disks (Henderson et al. 2007). It is not clear whether PSI–PSII megacomplexes exist only in vascular plants where the grana margin is well developed or exist widely in green plants, which have different thylakoid membrane structures.

Green plants survive under various light environments from terrestrial to marine deep-water environments (Leliaert et al. 2011). They have evolved various nonphotochemical quenching mechanisms to protect against photodamage, such as PsbS-dependent and Lhcsr-dependent quenching (Sylak-Glassman et al. 2014, Dinc et al. 2016, Kim et al. 2017). These mechanisms have a varied distribution among green plants (Niyogi and Truong 2013). One possible physiological function of PSI–PSII megacomplexes is to dissipate excess energy (Yokono et al. 2015). If this hypothesis is correct, the apparent ratio of PSI–PSII megacomplexes might differ among green plants grown in different light environments.

To elucidate the physiological function of PSI–PSII megacomplexes, we examined the structure of the PSI–PSII megacomplex of *Arabidopsis thaliana* using a newly developed electron microscopy technique and carried out time-resolved chlorophyll fluorescence analysis of various green plants. Our proposed structure of the PSI–PSII megacomplex suggests a direct connection between the PSI and PSII core antennas. This direct connection supports the fast energy transfer from PSII to PSI (~20 ps) previously observed in isolated PSI–PSII megacomplexes (Yokono et al. 2015). We found that PSI–PSII megacomplexes exist in almost all green plants including Streptophyta and Chlorophyta, although the levels differ among plants. We also found that green plants use the PSI–PSII megacomplex to dissipate excess energy via low-energy chlorophylls in PSI. Based on these results, we discuss the physiological function of PSI–PSII megacomplexes in green plants.

Results and Discussion

First, we determined the apparent ratio of PSI–PSII megacomplexes to all PSII complexes in various types of green plants with different terrestrial and aquatic habitats including land plants and green algae (Supplementary Fig. S1 and Supplementary Table 1). The results are summarized in **Fig. 1A**. In all land plants, about 50% of PSII was involved in PSI–PSII megacomplex formation, which is consistent with a previous result (Yokono et al. 2015). This ratio is also consistent with that of the PSII β-center (40–65%) determined by A. Melis using excitation light that can excite the PSII core directly (Melis 1975, Melis and Homann 1976, Melis and Akoyunoglou 1977, Melis and Thielen 1980). Conversely, some green algae accumulated a lower amount of PSI–PSII megacomplex (~25%). Interestingly, the apparent ratios of PSI–PSII megacomplexes did not reflect

A

	Species	Apparent ratio of PSI-PSII m.c.	Symbols in Fig.1B	Peak of low-energy chlorophyll
Streptophyta	*Amaranthus tricolor* (5 days)	44 (%)	N	742 (nm)
	Amaranthus tricolor (6 weeks)	54	O	742
	Arabidopsis thaliana	48	*	738
	Pinus thunbergii	45	M	740
	Setaria viridis	39	R	748
	Spinacia oleracea	52	L	744
	Zea mays (5 days)	47	P	740
	Zea mays (5 weeks)	38	Q	744
	Physcomitrella patens	48	K	730
	Klebsormidium flaccidum	20	E	724
	Mesostigma viride	28	F	725
	Penium margaritaceum	31	J	728
Chlorophyta	*Chlamydomonas reinhardtii*	24	C	716
	Haematococcus lacustris	27	D	718
	Chlorella variabilis	35	H	730
	Codium fragile	8.8	A	712
	Dichotomosiphon tuberosus	51	G	727
	Ulva pertusa	42	I	731
	Umbraulva japonica	26	B	714

B

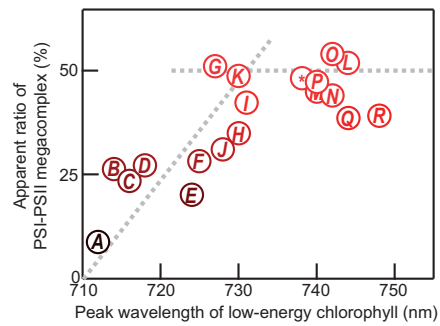

Fig. 1 The apparent ratio of PSI–PSII megacomplex in green plants (%). The stronger the red color, the higher the accumulation level of the PSI–PSII megacomplex. (A) The accumulation pattern seemed to reflect the optimal photon flux of the growth conditions rather than phylogeny. The ratios are summarized in Supplementary Table 1. The peak wavelength (nm) of low-energy chlorophyll fluorescence was obtained from the FDAS shown in Supplementary Fig. S1. The point with an asterisk reflects the *Arabidopsis* position obtained from a previous paper (Yokono et al. 2015). The periods in parentheses for *Amaranthus* and *Zea* indicate sampling times after seeding. (B) Relationship between the state of low-energy chlorophylls and the apparent ratio of PSI–PSII megacomplex in various green plants.

the phylogeny. For example, in class Ulvophyceae, we measured four species, *Codium fragile* and *Dichotomosiphon tuberosus* (Bryopsidales), *Ulva pertusa* and *Umbraulva japonica* (Ulvales). *C. fragile* accumulated only 8.8% of PSII as PSI–PSII megacomplexes, while *D. tuberosus* accumulated 51%. *U. japonica* accumulated 26%, while *U. pertusa* accumulated 42%. *C. fragile* and *U. japonica* have evolved to adapt to low-light conditions in marine deep water. Conversely, *D. tuberosus* and *U. pertusa* grow only in bright and shallow water. Note that all four species were preincubated under weak light for at least a few days before the measurement. Also note that the growth light conditions affected the ratio of PSI–PSII megacomplexes in land plants by about ±10% (**Fig. 2A**, **B**; Yokono et al. 2015), which is not be enough to explain the difference between 8.8% and 51%. Therefore, we assumed that the levels of PSI–PSII complexes were genetically determined to fit to the light environment during the evolution of green plants.

In addition to the difference in the apparent ratio of PSI–PSII megacomplexes, our time-resolved fluorescence analysis revealed variation of low-energy chlorophylls in PSI, also called red chlorophylls. All 16 species we examined possessed low-energy chlorophylls, but their lowest energy levels varied from 712 to 748 nm depending on the species (**Fig. 1** and Supplementary Fig. S1). All land plants contained low-energy chlorophylls showing fluorescence maxima longer than 730 nm (hereafter 'the deep trap'), some of which exist in LHCI (Morosinotto et al. 2003, Wientjes et al. 2012, Mazor et al. 2015). These organisms showed higher apparent ratio of PSI–PSII megacomplex as shown in **Fig. 1**. Conversely, in some green algae such as *C. fragile* and *U. japonica* the low-energy chlorophylls showed fluorescence maxima shorter than 720 nm, and these organisms accumulated less PSI–PSII megacomplex.

We examined whether the deep trap enhance high-light resistance of PSI. Changes in the absorbance of chlorophyll (678 nm) from isolated PSI were monitored after 1 h of high-light treatment (**Fig. 3A**, **B**). PSI–LHCI isolated from *Spinacia oleracea* showed a 738-nm fluorescence peak that originated from the deep trap (**Fig. 3C**, PSILHCI_738). The PSI–LHCI kept approximately 70% chlorophyll absorbance after high-light treatment (**Fig. 3A**, left). However, PSII–LHCII, LHCII and PSI cores, which does not possess the deep trap (Mullet et al. 1980), kept approximately 40% chlorophyll absorbance. This suggests

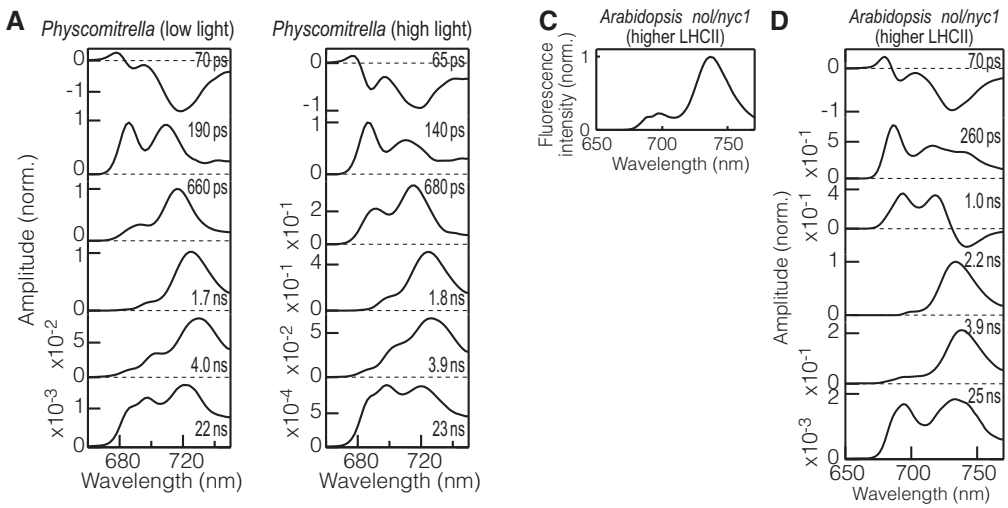

B

	Physcomitrella	
	low light	high light
Apparent ratio of PSI-PSII megacomplex	48%	31%

E

	Arabidopsis		
	ch1-1 (lower LHCII)	*wild type*	*nol/nyc1* (higher LHCII)
Apparent ratio of PSI-PSII megacomplex	54%*	48%*	35%

*These two values were determined from a previous report (Yokono et al. 2015).

Fig. 2 Effect of (A, B) growth light condition or (C–E) LHCII accumulation to the apparent ratio of PSI–PSII megacomplex. (A) FDAS of *P. patens* grown under low light (left, 30 μmol photons m^{-2} s^{-1}, the same figure shown in Supplementary Fig. S1K) and high light (right, 500 μmol photons m^{-2} s^{-1}). For high-light samples, decay curves were measured once with 2.4 ps and twice with 24.4-ps intervals. The PSI–PSII megacomplex ratio was calculated and is shown in (B). The different light conditions affected the PSI–PSII complex ratio, but not to a sufficient degree to explain the difference between 8.8% and 51%. (C) Steady-state fluorescence spectrum of a leaf of the *Arabidopsis nol/nyc1* double mutant, which accumulates a large amoutn of LHCII. The shape of the steady-state spectrum was similar to that of the wild type, indicating the accumulated LHCII bound to PSII and PSI in the proper ratio. Two independent experiments showed the same result. (D) FDAS of the *Arabidopsis nol/nyc1* double mutant. The PSI–PSII megacomplex ratio was calculated and is shown in (E). The PSI–PSII megacomplex ratio was partially influenced by the LHCII accumulation level. The *Arabidopsis ch1–1* mutant, which accumulates little LHCII, showed a higher PSI–PSII megacomplex ratio than the wild type. Conversely, the *Arabidopsis nol/nyc1* double mutant, which accumulates a lot of LHCII, showed a lower PSI–PSII megacomplex ratio than the wild type. Therefore, in green plants, PSI–PSII megacomplex formation may compete with additional LHCII binding to reaction centers.

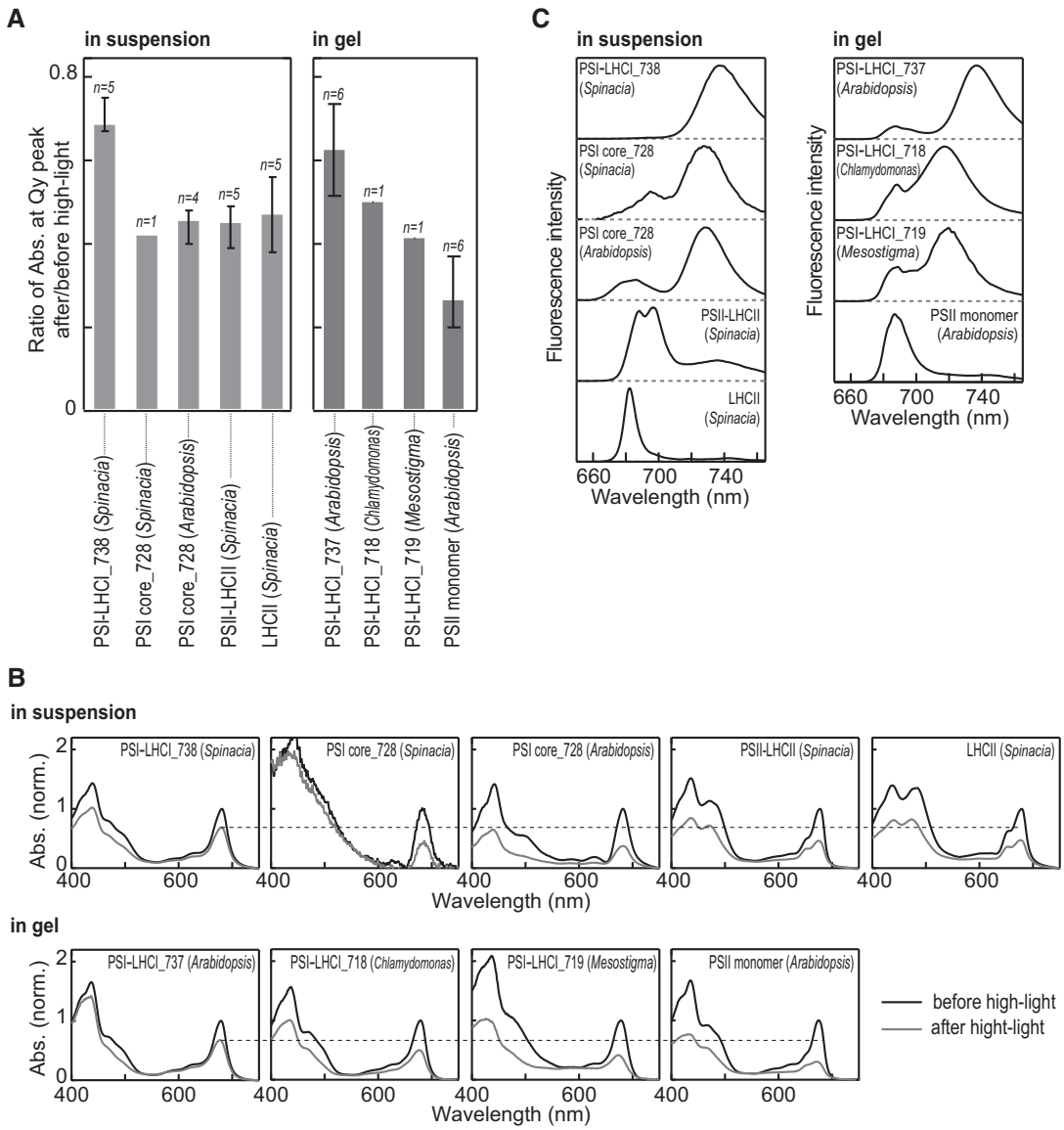

Fig. 3 High-light resistance of PSI with low-energy chlorophylls showing fluorescence maxima longer than 730 nm. (A) Sensitivity of isolated photosystem complexes to 60-min high-light exposure (2,000 µmol photons m^{-2} s^{-1}). Left: isolated complexes suspended in BTH buffer. Right: isolated complexes in CN-PAGE gel. The absorbance change was monitored at Qy peak before and after the high-light treatment, and the relative ratio was plotted. Error bars reflect the two extreme results from at least four independent measurements. The three-digit number in each sample name indicates the fluorescence peak wavelength of the low-energy chlorophyll of PSI in each sample shown in (C). (B) Absorption spectrum of isolated photosystem complexes before (black) and after (gray) the high-light exposure. The spectra were normalized at Qy peak in "before high-light". Note that the sample volume of the *Spinacia* PSI core was too small to cover the entire measurement beam area, so the signal was jaggy. (C) Fluorescence spectra of photosynthetic complexes at −196°C. Left, in suspension; right, in CN-PAGE gel.

that PSI with the deep trap has higher stability under high-light conditions than other chlorophyll protein complexes. This hypothesis is supported by a comparison of isolated PSI–LHCIs from various green plants, in which PSI–LHCI with the deep trap has higher stability (**Fig. 3A**, right). Collectively, the higher resistance to high-light treatment correlates with the deep trap of PSI, which is suggested to be involved in various energy dissipation processes (Shubin et al. 1995, Schlodder et al. 2011, Ballottari et al. 2014).

A previous report suggested that once $P700^+$ accepts excitation energy, the energy is converted to heat within 0.2 ps (Trissl 1997). However, $P700^+$ has absorption maxima around 800 nm (Stewart et al. 1999); therefore, bulk chlorophylls that emit around 680 nm cannot transfer energy directly due to the lack of a Förster overlap integral (Shubin et al. 1995). Therefore, the deep trap is required to transfer excitation energy to $P700^+$ from normal chlorophylls, and the quenching efficiency of the process is improved when the energy level of the deep trap is lower (Schlodder et al. 2011).

Next, we examined the correlation between the apparent ratio of the PSI–PSII megacomplex and the energy level of the low-energy chlorophyll of PSI (**Fig. 1B**). We observed a

correlation with a coefficient of 0.77, suggesting a relationship between the function(s) of the PSI–PSII megacomplex and the deep trap in PSI. Here, PSI–PSII megacomplexes isolated from *A. thaliana* showed 23% faster fluorescence decay of the deep trap under $P700^+$ conditions than P700 conditions (**Fig. 4**), suggesting quenching of excitation energy via energy transfer from the deep trap to $P700^+$ in the PSI–PSII megacomplex.

In addition, the low-energy chlorophylls enhance the formation of xanthophyll radical cations, which also dissipate excess energy in *A. thaliana* (Ballottari et al. 2014). Therefore, one of the physiological functions of the PSI–PSII megacomplex is the quenching of excess energy by PSI via the deep trap. When the PSII reaction center is closed in the PSI–PSII megacomplex, excess energy harvested by PSII can be quenched by PSI (Yokono et al. 2015).

There were two phases in the relationship between the relative amount of PSI–PSII megacomplex and the energy level of low-energy chlorophyll (**Fig. 1B**). The relative amount of PSI–PSII megacomplex increased up to approximately 50% along with a decline in the energy level of low-energy chlorophyll (longer wavelength), and then seemed to remain at approximately 50%. One phase indicates that the species with the deep trap prefer the PSI–PSII megacomplex. The other phase was mainly observed in land plants, which accumulated about 50% of PSII as the PSI–PSII megacomplex. This phase may reflect the need for PSII that does not transfer excitation energy to PSI to maintain linear electron transfer.

Our present results show different levels of PSI–PSII megacomplexes among green plants. For example, *Chlamydomonas* has a very low megacomplex ratio, although its PSI and PSII have similar protein compositions to those of land plants. To determine the reason for the differences in PSI–PSII megacomplex levels among organisms and for the fast energy transfer in the PSI–PSII megacomplex, we needed structural information. In our preliminary experiments, electron micrograph images of the megacomplexes were heterologous (Supplementary Datasets and Supplementary Fig. S2A). Thus, various assembly stages and/or assembly types of megacomplexes might exist in the thylakoid membranes. However, we cannot exclude the possibility that the purification processes partially affected the heterogeneity, because digitonin can remove some LHCII from reaction centers (Benson et al. 2015, Bressan et al. 2018). The widely used single-particle analysis method could not be applied to the heterologous images. We thus developed an appropriate method to our study, in which we applied a new fitting strategy to the PSI–PSII megacomplex particles (Supplementary Fig. S3 and Supplementary Text 2) based on the principle of global target analysis of time-resolved spectroscopy data (see the Materials and Methods section). As a result, we successfully constructed an image of the PSI–PSII megacomplex by incorporating images of 88% of the particles (**Fig. 5A**) using a double row guide model (Supplementary Fig. S3C, right). In the reconstructed image (**Fig. 5A**), a single row was prominent (Supplementary Fig. S3C, left). This is because 71% of particles could be explained by the single row model, and only 17% (88−71) of particles required the double row model to fit. Therefore, at this stage, we propose the single row model as a model of the PSI–PSII megacomplex in *A. thaliana* (**Fig. 5B**). The reconstructed image indicates that a PSII dimer is directly sandwiched between two PSIs with 2-fold rotational symmetry in the majority of PSI–PSII megacomplexes. The direct binding of PSII and PSI core antennas should enable the fast excitation energy transfer (~20 ps) between PSII and PSI (Yokono et al. 2015). Based on the model, we determined the following parameters for the PSI–PSII megacomplex; PSI:PSII = 1:1 and chlorophyll *a*/*b* ratio = 3.6 ± 0.4 (Supplementary Fig. S3C and Supplementary Datasets), which are consistent with our previous report (Yokono et al. 2015). Several LHCII trimers were found around the megacomplex, which is consistent with our previous data that a lot of LHCII is contained in the megacomplex (Supplementary Figs. S7, S11 in Yokono et al. 2015). However, the image does not necessarily indicate that the megacomplex is completely surrounded by LHCs, because the numbers detected (observed frequencies) were different among various LHCs and also lower compared with the core complexes of both photosystems (Supplementary Fig. S3C). The three most frequently observed LHCIIs were M- and S-trimers for PSII (positions 1 and 3 in **Fig. 5B**; Caffarri et al. 2009) and L-trimers for PSI (position 2 in **Fig. 5B**; Kouril et al. 2005). On average, our analysis showed that 3.3 LHCII trimers bound to one PSI, which is in good agreement with recent results [3.2 ± 0.9 in (Bell et al. 2015) and approximately 2.4 in (Bos et al. 2017)]. Additionally, 60% of the trimers bound via the LHCI belt, which explains why LHCI mutation decreases LHCII binding to PSI (up to 69%; Benson et al. 2015). Recently, LHCII binding to the LHCI belt was reported in *A. thaliana* (Yadav et al. 2017), and the binding positions are consistent with our model (Supplementary Fig. S4A). The binding pattern between

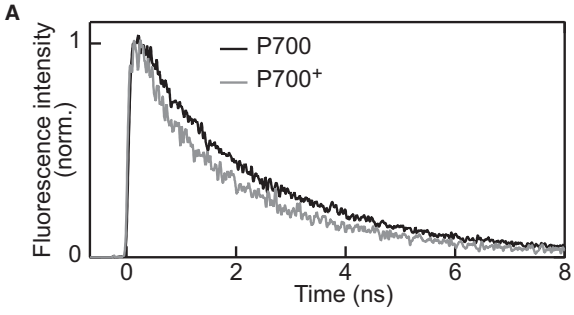

B

	τ_{mean}	Lifetime (Amplitude)		
P700	2.29 ns	45 ps (-93%)	0.23 ns (40%)	2.42 ns (60%)
$P700^+$	1.76 ns	83 ps (-55%)	0.19 ns (57%)	1.95 ns (43%)

Fig. 4 $P700^+$ accerelates energy dissipation in the PSI–PSII megacomplex. PSI–PSII megacomplex was incubated with 1-mM ferricyanide and 0.1-mM DCMU for 10 min at 4°C and frozen under illumination to achieve $P700^+$ condition. (A) Fluorescence decay curve of the PSI–PSII megacomplex isolated from *A. thaliana*. Fluorescence was monitored at 735 nm at −196°C. Lifetimes and their amplitudes are summarized in (B). Positive and negative amplitudes indicate decay and rise components, respectively. Mean lifetime became 23% faster in $P700^+$ condition than in P700 condition.

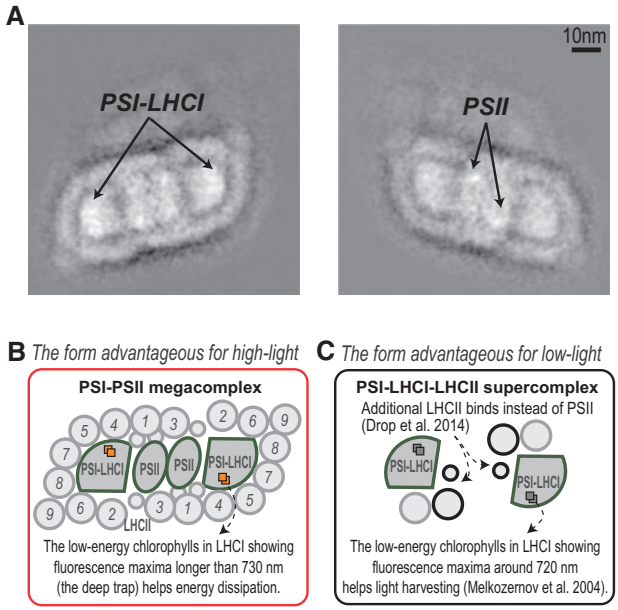

Fig. 5 A hypothetical model of the PSI–PSII megacomplex in green plants. (A) Averaged images of the PSI–PSII megacomplex of *A. thaliana* constructed from all successfully fitted particles. The averaged image viewed from the Fe–S cluster of PSI showed a dense region in PSI region (left), while the image viewed from opposite side showed a dense region in PSII region (right). Averaged images with the exception of small particles (<1,200 kDa) showed the same result (Supplementary Fig. S2B). (B) A hypothetical scheme of the PSI–PSII megacomplex in higher plants based on the averaged images of the PSI–PSII megacomplex from *A. thaliana*. One PSII dimer was directly sandwiched by two PSI–LHCI with two times rotational symmetry, and additional LHCII surrounded peripherally. Large and small gray circles indicate trimer and monomer of LHCII, respectively. Digit on each LHCII trimer reflect ranking of binding probability. Orange squares are the low-energy chlorophylls in LHCI showing fluorescence maxima longer than 730 nm (the deep trap), and helps energy dissipation. We note that stress conditions could induce different binding patterns between PSI and PSII, such as a LHCII-bridged type connection (Grieco et al. 2015). (C) Model of PSI–LHCI–LHCII of *C. reinhardtii* proposed previously (Drop et al. 2014). Low-light adaptable green plants may sacrifice the direct binding between PSI and PSII in favor of the additional LHCII (black circles) binding to PSI. Gray squares are low-energy chlorophylls in LHCI showing fluorescence maxima around 720 nm, and helps light harvesting.

PSI and PSII seems consistent with the edge shapes of their structures (Supplementary Fig. S4B). Based on the image, we assume that the PSII binding site is close to PsaH, PsaI and PsaB in PSI. This binding site is on the same side that the additional LHCII binds to PSI in low-light adaptable green algae (**Fig. 5C**) (Drop et al. 2014). For PSII, the PSI binding site is also occupied by an additional LHCII in low-light adaptable green algae (Tokutsu et al. 2012). Low-light adaptable species may be able to increase their effective antenna size at low cost, which prevents the formation of PSI–PSII megacomplexes. The competitive relationship between PSI and PSII megacomplex formation and LHCII accumulation was confirmed using *A. thaliana* mutants (**Fig. 2E**). Note that other factors such as a biased ratio of PSI to PSII in a cell could affect the PSI–PSII megacomplex ratio (Q and R in **Fig. 1**, discussed in Supplementary Text 1).

When LHCII is accumulated in vascular plants, it forms a head-to-head connection via divalent cations and facilitates grana stacking (Kirchhoff et al. 2003, Schaller et al. 2014, Kaňa 2016). Thus, more than half of LHCII exists in the grana core and is independent from PSI (Suorsa et al. 2014). Consequently, PSI might have the opportunity to form a direct connection to PSII, which is required for the fast energy transfer from PSII to PSI. If this hypothesis is correct, grana stack formation may have two photoprotective roles: (1) enhancing the direct connection between PSI and PSII to protect PSII via the deep trap in PSI, and (2) mediation of PsbS, LHCII and ΔpH-related non-photochemical quenching (NPQ) (Correa-Galvis et al. 2016). The latter is part of the P700 oxidation system, which enhances accumulation of $P700^+$ in PSI (Takagi et al. 2016, Takagi et al. 2017). As already discussed, in the PSI–PSII megacomplex, excitation energy from PSII is transferred to $P700^+$ via the deep trap and converted to heat. Therefore, the two photoprotective roles could have a synergistic effect in energy dissipation. Further study is required to verify this hypothesis.

Our results suggest that green plants use the PSI–PSII megacomplex to dissipate excess energy via the deep trap in PSI. In evolutionary history, the deep trap was first acquired by cyanobacteria (Shubin et al. 1995, Schlodder et al. 2011). Some cyanobacteria generate the deep trap by trimerization of PSI, and a phycobilisome antenna bridges PSII and the trimeric form of PSI (Liu et al. 2013). The ancestor of green algae acquired the photosystems from a cyanobacterial symbiont. However, ancestral green algae lost both phycobilisomes and the deep trap (Falkowski et al. 2004, Kunugi et al. 2016), which might have been related to both nutrient and light limitation. Green algae couple many LHCIIs with reaction centers to increase the light-harvesting efficiency at low cost (Tokutsu et al. 2012, Drop et al. 2014). The low-energy chlorophylls in LHCI showing fluorescence maxima around 720 nm transfer their energy to P700 via an uphill pathway (Melkozernov et al. 2004), which also increases light-harvesting efficiency. Later, some green algae acquired the deep trap by LHCI modification. The deep trap contributes to the high stability of PSI under high-light conditions. These species may then have been able to accumulate additional PSII as PSI–PSII megacomplexes as a safe backup to adapt to strong sunlight (Yokono et al. 2015).

Materials and Methods

Plant materials for time-resolved fluorescence measurements

To clarify the interspecies distribution of the PSI–PSII megacomplex in green plants, we measured 20 samples from 16 species of Chlorophyta and Streptophyta. Harvested plants were immediately frozen in optical quartz tubes to measure time-resolved fluorescence.

Amaranthus tricolor *and* Zea mays. *A. tricolor* and *Z. mays* seeds were purchased from TAKII & Co., Ltd. (Kyoto, Japan), and grown at 22°C under long-day conditions (14 h, 50 μmol photons m^{-2} s^{-1}; white fluorescent lamp). Five days after sowing, some cotyledons were harvested and immediately frozen

in optical quartz tubes to measure time-resolved fluorescence (samples 'N' and 'P' in **Fig. 1**, Supplementary Fig. S1, and Supplementary Table 1). The remaining plants were moved to higher-light conditions (3 h, 50 μmol photons m^{-2} s^{-1}; 8 h, 300 μmol photons m^{-2} s^{-1}; 3 h, 50 μmol photons m^{-2} s^{-1}; halogen lamp) about 4 weeks after sowing. Mature leaves were harvested 5–6 weeks after sowing to measure time-resolved fluorescence (samples 'O' and 'Q' in **Fig. 1**, Supplementary Fig. S1, and Supplementary Table 1).

Setaria viridis, Pinus thunbergii and Spinacia oleracea. Mature leaves of *S. viridis* and *P. thunbergii* were harvested from the campus of Kobe University (Hyogo, Japan) on April 12, 2015. *S. oleracea* leaves were harvested on April 11, 2015 from plants purchased on the same day from a greengrocery near Kobe University.

Arabidopsis thaliana. The Δ*nol/nyc1* double mutant of *A. thaliana* (Columbia ecotype; Horie et al. 2009) was grown at 22°C under short-day conditions (8 h light, 50 μmol photons m^{-2} s^{-1}, white fluorescent lamp) as described previously (Yokono et al. 2015). After about 8 weeks, the plants were moved to dark conditions for 10 days. After the treatment, some leaves became yellow, but others still looked fresh and green. The green leaves showed a low chlorophyll *a*/*b* ratio (~1.7), and were used to measure the steady-state fluorescence spectrum and the time-resolved-fluorescence spectrum. The wild-type Columbia ecotype *A. thaliana* was grown at 22°C under short-day conditions (8 h light, 50 μmol photons m^{-2} s^{-1} or 500 μmol photons m^{-2} s^{-1}) as described previously (Yokono et al. 2015).

Physcomitrella patens (Bryophyta). *P. patens* protonemata were cultured basically according to a previous report (Takabayashi et al. 2016). In brief, on a layer of cellophane overlaid on BCDAT agar medium at 25°C under white light (16 h light, approximately 30 μmol photons m^{-2} s^{-1}). About 4 days after transplanting, some protonemata were collected as a low-light sample; the remaining samples were high light treated for 4 days with cold spot fiber optics (16 h light, 500 μmol photons m^{-2} s^{-1}; PCS-UMX250; NPI, Tokyo, Japan) and collected as a high-light sample.

Ulvophycean algae: C. fragile, U. pertusa, U. japonica and Dichotomosiphon tuberosus. The macrophytic and benthic marine green algae *C. fragile*, *U. pertusa* and *U. japonica* were collected from the seashore around Awaji Island (Hyogo, Japan) and maintained under weak white light for several days at 20°C. The freshwater and benthic green alga *D. tuberosus* was collected in a shallow waterway from spring water in Ginowan (Okinawa, Japan) and cultured as a unialgal strain in artificial medium at the laboratory of Kobe University.

Charophyta, Mesostigmatophyta, Chlorophyceae and Trebouxiophyceae. *Klebsormidium flaccidum* (NIES-2285), *Mesostigma viride* (NIES-296), *Penium margaritaceum* (NIES-303), *Chlorella variabilis* (NIES-2541) and *Haematococcus lacustris* (NIES-144) were obtained from the National Institute for Environmental Studies, Ibaraki, Japan. *Chlamydomonas reinhardtii* [CC-1931(arg7)] was provided by the Chlamydomonas Genetic Centre (Duke University, Durham, NC, USA; Tanaka et al. 1998). The mutant is cell wall-less, so we can isolate the thylakoid very quickly. Each was inoculated into 100 ml of liquid medium in 200 ml Erlenmeyer flasks and grown at 24.5°C under a 14 h photoperiod of 40 μmol photons m^{-2} s^{-1} as described previously (Kunugi et al. 2016). Cultures in the late logarithmic phase were collected to measure time-resolved fluorescence.

Steady-state and time-resolved fluorescence measurements

The steady-state fluorescence spectrum at −196°C was measured using an F-2500 spectrophotometer (Hitachi, Tokyo, Japan; Yokono et al. 2015). The excitation wavelength was 440 nm. The optical slit widths for excitation and emission were 10 and 2.5 nm, respectively.

Time-resolved fluorescence decay curves at −196°C were measured as described previously (Yokono et al. 2015) but using a diode laser (PIL040X, 408 nm) controlled by an EIG2000DX-40 (Advanced Laser Diode System) as an excitation source. The laser intensity was set to ≤0.1 nJ/pulse. All experiments were replicated at least twice. The reproducibility of the decay curves was verified, and the curves were summed and the kinetics were analyzed (Yokono et al. 2015). Fluorescence decay-associated spectra (FDAS) were constructed, and the PSI–PSII megacomplex ratio was determined as described previously (Yokono et al. 2011, Yokono et al. 2015) and summarized in the next section. Potential error margins were estimated using 11 *A. thaliana* leaves harvested from 11 different individuals (S_1 energy level of the low-energy chlorophyll, SD 0.9 nm; PSI–PSII megacomplex ratio, SD 6.3%). PSI–PSII megacomplex samples for fluorescence measurement were prepared as described previously (Yokono et al. 2015). Samples with P700 in the oxidized state were prepared according to a previous report with slight modification (Schlodder et al. 2011). In brief, samples were incubated with 1-mM ferricyanide and 0.1-mM DCMU for 10 min at 4°C and frozen under illumination.

Estimation of apparent ratio of the PSI–PSII megacomplex

Delayed fluorescence (DF) (~20 ns) originates from charge recombination at the PSII reaction center (Mimuro et al. 2007), so the DF spectrum reflects the excitation energy distribution after direct excitation of the PSII reaction center (Yokono et al. 2011, Yokono et al. 2015). Therefore, a peak in the DF spectrum in the PSI wavelength region suggests excitation energy transfer from the PSII reaction center to PSI. We estimated the apparent ratio of PSII present in the PSI–PSII megacomplex for all PSII as follows:

1. We first read the amplitude of the DF at the PSII peak and PSI peak from the sixth lifetime component of the FDAS (A_{PSII}, A_{PSI}).
2. As the vibrational band of PSII fluorescence affects the PSI wavelength region, we estimated its effect from the fluorescence spectrum of isolated PSII dimers (Tomo et al. 2009). It depended on the wavelength, but typically approximately 20% of A_{PSII} represented the vibrational band intensity in the PSI wavelength region. In this case, the corrected DF intensity at the PSII and PSI peaks is $DF_{PSII} = A_{PSII}$ and $DF_{PSI} = A_{PSI} - 0.2 \times A_{PSII}$. These values are summarized in Supplementary Table 1.
3. The DF intensities (DF_{PSII} and DF_{PSI}) reflect two factors, the excitation energy distribution and excited state lifetime. If the events of acceptance and dissipation of excitation energy are independent, the DF intensity can be expressed as a product of the two factors. For example, if twice the amount of energy is transferred from PSII to PSI, DF_{PSI} becomes two times stronger. If the excited state lifetime at the PSI wavelength is twice as long (such as in the case of NPQ deactivation), DF_{PSI} becomes two times stronger. If both events occur, DF_{PSI} becomes four times stronger.
4. First, we considered the excitation energy distribution. Here, energy transfer from PSII to PSI in the PSI–PSII megacomplex occurs fast (~20 ps; Yokono et al. 2015), so we assumed that almost all of the excitation energy of PSII was transferred to PSI in the PSI–PSII megacomplex at −196°C. In this case, the excitation energy distribution mainly reflects the number of complexes: (i) DF_{PSII} reflects the number of PSIIs that do not form physical connection to PSIs ($N_{\_independent\_PSII}$), and (ii) DF_{PSI} reflects number of PSIIs that exist as PSI–PSII megacomplexes ($N_{\_PSI-PSII}$).
5. Next, we considered the excited state lifetime. The excited state lifetime can be assumed from the mean lifetime of normal (not delayed) fluorescence, which is caused by direct laser excitation, in the time range 0–7 ns (Yokono et al. 2011).

The normal fluorescence decay kinetics can be expressed from the first to fifth lifetime components of the FDAS excluding negative amplitudes.

$$F(t) = \sum_{i=1}^{5} Amp_i \times e^{\frac{-t}{Tau_i}}$$

Amp_i and Tau_i is the positive amplitude and its lifetime in each lifetime component at a given wavelength, respectively. The mean lifetime (τ) was calculated from $F(t)$.

$$\tau = \frac{\int_0^\infty t \times F(t)dt}{\int_0^\infty F(t)dt}$$

Mean lifetimes at the PSII and PSI peak wavelengths (τ_{PSII}, τ_{PSI}) are summarized in Supplementary Table 1.

1. Finally, the relationship between the DF intensity (DF_{PSII}, DF_{PSI}), number of PSII complexes ($N_{\_independent\_PSII}$, $N_{\_PSI-PSII}$) and mean lifetime (τ) can be expressed as follows.

$$DF_{PSII} = \alpha \times N_{\_independent\_PSII} \times \tau_{PSII} \quad DF_{PSI} = \alpha \times N_{\_PSI-PSII} \times \tau_{PSI}$$

Here, α reflects the probability of charge recombination within a PSII reaction center after it accepts excitation energy. Then, the number of PSII complexes can be expressed as follows.

$$N_{\_independent\_PSII} = \frac{DF_{PSII}}{\alpha \times \tau_{PSII}}$$

$$N_{\_PSI-PSII} = \frac{DF_{PSII}}{\alpha \times \tau_{PSI}}$$

The apparent ratio of PSII assembled into PSI–PSII megacomplexes can be expressed as follows.

$$100 \times \frac{N_{\_PSI-PSII}}{N_{\_independent-PSII}+N_{\_PSI-PSII}} = 100 \times \frac{\frac{DF_{PSI}}{\tau_{PSI}}}{\frac{DF_{PSII}}{\tau_{PSII}}+\frac{DF_{PSI}}{\tau_{PSI}}}$$

If all the assumptions used so far are correct, this apparent ratio can be considered the real ratio of the PSI–PSII megacomplex.

Isolation of photosynthetic complexes for evaluation of high-light stability

Isolation of PSI–LHCI, LHCII and BBY particles (PSII–LHCII enriched fraction) from S. oleracea. PSI–LHCI and LHCII of *S. oleracea* were isolated as described previously (Hirashima et al. 2006). In brief, green leaves were homogenized in a blender with ice-cold buffer containing 0.35 M sucrose, 50-mM Tricine/NaOH (pH 8.0), and 5-mM EDTA. The homogenate was filtered through a layer of Miracloth (Merck Millipore Co.). A pellet was obtained by centrifugation at 10,000 × *g* for 10 min. The pellet was washed with 5-mM EDTA (pH 8.0) twice. The washed membranes were solubilized in 0.8% Triton X-100 to a final chlorophyll concentration of 0.8 mg ml^{-1} and centrifuged at 110,000 × *g* for 30 min at 4°C. The green supernatant was loaded onto a linear 0.1–0.7-M sucrose density gradient containing 0.08% Triton X-100 and centrifuged at 110,000 × *g* for 14 h at 4°C. A green band was collected from the sucrose density gradient, and LHCII was purified by adding $MgCl_2$ and KCl (Burke et al. 1978); the chlorophyll *a*/*b* ratio was 1.3. PSI particles were obtained as a nonfluorescent green pellet; the chlorophyll *a*/*b* ratio was 6.8. The pellets were suspended in 25BTH20G buffer [25-mM BisTris/HCl pH 7.0, 20% (w/v) glycerol, 0.25 mg ml^{-1}, Pefabloc SC, 10-mM sodium fluoride; Järvi et al. 2011], and stored at −196°C until spectroscopic measurement.

BBY particles (PSII–LHCII enriched fraction) were isolated by a combination of Triton X-100 and centrifugation (Kuwabara and Murata 1982). Green leaves were homogenized in a blender with ice-cold buffer containing 0.1-M sucrose, 0.2-M NaCl and 50-mM Na/K phosphate buffer (pH 7.4). The homogenate was filtered through two layers of Miracloth. A pellet was obtained by centrifugation at 3,000 × *g* for 5 min. The pellet was resuspended in another medium containing 0.3-M sucrose, 50-mM NaCl and 50-mM Na/K phosphate buffer (pH 6.9) at a chlorophyll concentration of 2.5 mg ml^{-1}. An aqueous solution of Triton X-100 (20% w/v) was added to the suspension with stirring until the ratio of Triton X-100 to chlorophyll became 20:1 (w/w). After incubation for 1 min, the suspension was centrifuged at 1,000 × *g* for 2 min, the pellet was discarded, and the supernatant was centrifuged at 48,000 × *g* for 20 min. The pellet was solubilized again in Triton X-100 under the same conditions. After incubation for 1 min, the suspension was centrifuged at 48,000 × *g* for 20 min. The resultant pellet was suspended in 25BTH20G buffer (Järvi et al. 2011), and stored at −196°C until spectroscopic measurement. The chlorophyll *a*/*b* ratio was 1.8. Properties of the BBY particles are summarized in Supplementary Fig. S6.

Isolation of the PSI core from the A. thaliana ch1–1 *mutant.* The *A. thaliana ch1–1* mutant accumulates little LHCI or LHCII; therefore, we isolated the PSI core from the mutant with a similar procedure to that described above. In brief, the plant was grown at 22°C under short-day conditions (8 h light, 50 μmol photons m^{-2} s^{-1}, white fluorescent lamp) as described previously (Yokono et al. 2015). After about 8 weeks, the plant was harvested and homogenized with ice-cold buffer containing 0.35-M sucrose, 50-mM Tricine/NaOH (pH 8.0) and 5-mM EDTA. The homogenate was filtered through a layer of Miracloth (Merck Millipore Co.). A pellet was obtained by centrifugation at 12,000 × *g* for 10 min. The pellet was washed with 5 mM EDTA (pH 8.0) twice. The washed membranes were solubilized in 0.8% Triton X-100 to a final chlorophyll concentration of 0.8 mg ml^{-1} and centrifuged at 190,000 × *g* for 30 min at 4°C. The green supernatant was loaded onto a linear 0.1–0.7-M sucrose density gradient containing 0.08% Triton X-100 and centrifuged at 110,000 × *g* for 18 h at 4°C. PSI particles were obtained as a nonfluorescent green pellet (Mullet et al. 1980). The resultant pellets were suspended in 25BTH20G buffer (Järvi et al. 2011), and stored at −196°C until spectroscopic measurement.

Isolation of the PSI core from S. oleracea. The PSI core was purified from isolated PSI–LHCI as described previously (Mullet et al. 1980). In brief, the isolated PSI–LHCI was solubilized in 0.45% Triton X-100 to a final chlorophyll concentration of 0.2 mg ml^{-1} for 30 min at 20°C. The green supernatant was loaded onto a linear 0.1–1.0-M sucrose density gradient containing 0.35% Triton X-100 and centrifuged at 100,000 × *g* for 9 h at 4°C. A green band was collected, and diluted 1:1 with ultrapure water. The mixture was centrifuged at 200,000 × *g* for 1 h at 4°C. The soft pellet was suspended in ultrapure water, and centrifuged at 200,000 × *g* for 1 h at 4°C. The resultant pellets were suspended in 25BTH20G buffer (Järvi et al. 2011), and stored at −196°C until spectroscopic measurement.

Isolation of PSI–LHCI from A. thaliana, M. viride and C. reinhardtii by lpCN-PAGE. Thylakoid membranes were isolated as described previously (Yokono et al. 2015, Kunugi et al. 2016). The thylakoid membranes were solubilized with 1% n-dodecyl-β-D-maltoside at 0.5 mg chlorophyll per milliliter in 25BTH20G buffer for 1 min on ice. lpCN-PAGE was performed as described previously (Yokono et al. 2015). Bands of PSI–LHCI were excised, and used for spectroscopic measurements immediately.

Evaluation of the high-light stability of isolated photosynthetic complexes by measuring absorption spectra

Recent reports suggest that PSI–LHCI complexes with photodamaged iron–sulfur clusters can participate in excitation energy dissipation (Tiwari et al. 2016). This result suggests that PSI–LHCI itself, without an electron donor or acceptor, can perform energy dissipation. This kind of energy dissipation mechanism can be evaluated by absorption measurement during high-light irradiation. If a PSI–LHCI has low-energy dissipation capacity, the formation of the triplet excited state of chlorophyll and radical species will not be suppressed efficiently. Subsequently, the PSI–LHCI will be rapidly destroyed by the radical species, which can be detected by the reduced absorption intensity of PSI–LHCI.

Steady-state absorption spectra at room temperature were measured using a light-guided multichannel photodiode array detector (EPP2000C-XR, slit width 50 μm, StellarNet-Inc., USA) equipped with a tungsten lamp (SL1), optical fibers (F600-UV-VIS-SR) and a collimating lens (Lens-QCol). The obtained data were analyzed with Igor Pro (ver. 6.3, WaveMetrics).

PSI–LHCI, the PSI core, LHCII and BBY particles (PSII–LHCII enriched fraction) isolated from *S. oleracea* were diluted with 25BTH20G buffer to 5-μg

chlorophyll per milliliter. The PSI core isolated from *A. thaliana* was also diluted the same way. Each sample was sealed in an optical cell and purged with nitrogen. Absorption spectra were measured at 20°C and then high-light treatment was applied for 1 h at 20°C with cold spot fiber optics (2,000 μmol photons m^{-2} s^{-1}). After the treatment, the absorption spectra were measured again, and the relative absorbance at 678 nm was calculated.

Gel bands of PSI–LHCI isolated from *A. thaliana*, *M. viride* and *C. reinhardtii* were sealed in optical cells with a piece of wet filter paper to prevent desiccation, and purged with nitrogen. Absorption spectra were measured at 20°C and then high-light treatment was applied for 1 h at 20°C with cold spot fiber optics (2,000 μmol photons m^{-2} s^{-1}). After the treatment, the absorption spectra were measured again, and the relative absorbance at 678 nm was calculated.

Isolation of the PSI–PSII megacomplex for electron micrographs

Thylakoid membranes were isolated from *A. thaliana* grown at 22°C under short-day conditions (16 h, dark; 8 h light, 50 μmol photons m^{-2} s^{-1}), and solubilized in 25BTH20G buffer with 1% digitonin (Sigma-Aldrich Japan, Tokyo) at 18°C (Järvi et al. 2011; Rantala et al. 2017; Yokono et al. 2015). Under these conditions, grana margins and stroma lamellae are solubilized. We first tried to isolate the PSI–PSII megacomplex by lpCN-PAGE from the solubilized fraction (Kouřil et al. 2014; Yokono et al. 2015). The gel band containing PSI–PSII megacomplexes (w1 band) was excised from the lpCN-PAGE gel, chopped up and placed in an Eppendorf tube with 50 μl of an extraction buffer (0.05% digitonin, 50-mM BisTris/HCl, pH 7.0 at 4°C). A previous report suggested that a complex with PSI and NAD(P)H dehydrogenase complex (PSI-NDH complex) (~30 nm diameter, ~1,500 kDa) could be eluted from the gel band after 2 h (Kouřil et al. 2014). However, a few broken particles were observed even after overnight elution in the case of the PSI–PSII megacomplex band. We suspected that the PSI–PSII megacomplex was too large (>2,400 kDa), and could easily become stuck in pores of the polyacrylamide gel.

Thus, we tried to isolate the PSI–PSII megacomplex by clear-native agarose gel electrophoresis (CN-AGE). The procedures are summarized in Supplementary Fig. S5. In brief, the cathode buffer (50-mM Tricine, 15-mM BisTris/HCl pH 7.0 at 4°C, 0.05% sodium deoxycholate) and the anode buffer (50-mM BisTris/HCl pH 7.0 at 4°C) were the same as in a previous report (Yokono et al. 2015). The gel buffer contained 0.05% digitonin, 20% glycerol and 50-mM BisTris/HCl pH 7.0 at 4°C.

Agarose cannot be bonded to glass plates, so we built a composite frame with an acrylamide gel and a filter paper (Advantec, No. 590) sandwiched by mini-gel glass plates. The total acrylamide concentration was 12.5% with a ratio of bisacrylamide to total acrylamide of 3%. The frame was solidified at 40°C, and then floated on hot ion-exchanged water (~80°C).

For the separation gel, 3% agarose gel was used. Agarose was cast in the floated frame and solidified for approximately 12 h. In a 1% gel, all loaded samples flowed through before it was separated, probably because the pore size was too large. In a 4% gel, the PSI–PSII megacomplex did not enter the separation gel.

For the sample gel, the total acrylamide concentration was 3%, with a ratio of bisacrylamide to total acrylamide of 20%, which was the same as in a previous report [stacking gel in (Yokono et al. 2015)]. The sample gel was polymerized at 30°C for 45 min.

Electrophoresis was performed at 4°C at 75 V for 60 min and 200 V for about 120 min. The cathode buffer was replaced every hour. During the 75-V stage, all loaded samples passed through the sample gel and entered into the separation gel. We examined three types of agarose (J234, Amresco, strength = 500 g cm^{-2} at 1.5%; NE-AG01 FastGene, strength = 1,000 g cm^{-2} at 1%; 3:1 HRB, Amresco, strength = 2,000 g cm^{-2} at 1.5%). J234 and 3:1 HRB seemed to give a better separation.

At the 200-V stage, the separation gel was axially compressed gradually, so the pore size became smaller. Finally, the gel was compressed about two times in the latter stage of electrophoresis, and the separation became better. When the electrophoresis was finished, the compressed gel returned to its original size, and the pore size may also have increased. The excised band was frozen in liquid nitrogen immediately, and the fluorescence spectrum was measured to verify energy transfer to PSI (Supplementary Fig. S5G). The band showed exactly the same profile as the w1 band (larger PSI–PSII complex) published previously (Yokono et al. 2015), where the fluorescence spectrum showed a PSI peak despite the existence of PSII and LHCII, and suggesting efficient energy transfer from LHCII and PSII to PSI. It was then melted in the extraction buffer (0.05% digitonin, 50-mM BisTris/HCl, pH 7.0 at 4°C) at 4°C. A green solution was observed after about 1 h. The solution was diluted with the extraction buffer, applied to a glow-discharged carbon-coated copper grid (#300) for 1 min, and negatively stained for 30 s three times with 2% uranyl acetate on ice. Electron microscopy was performed on a H-7650 electron microscope (Hitachi) operating at 80 kV. After four independent sample separations and grid preparations, electron micrographs of 612 particles were obtained in total, and analyzed as described below using Mathematica (ver. 7, Wolfram Research) and Photoshop (CS5.1, Adobe systems).

Jigsaw puzzle approach using a global target analysis strategy

We examined the structure of the PSI–PSII megacomplex in *A. thaliana*. Electron micrographs showed that the particles had structural heterogeneity (Supplementary Fig. S2A and Supplementary Datasets), probably because of the varied binding patterns of peripheral LHCIIs to the PSI–PSII megacomplex and/or various assembly states, but we found shared structures in these particles. Because of the nature of the structural heterogeneity of the PSI–PSII megacomplex, the structural variation is so large that it cannot be analyzed by ordinary single-particle analysis (i.e. 18 LHCII binding sites with two times rotational symmetry should make $2^{18}/2$ variations). It is also important to know the frequencies of each component, such as LHC and PSI particles, in the megacomplexes. Therefore, we applied a new fitting strategy to the PSI–PSII megacomplex particles (Supplementary Fig. S3) based on a strategy of global target analysis of time-resolved spectroscopy data (Holzwarth 1996). This strategy could extract the minimum number of unknown parameters (in this case, subunits compositions and binding patterns) required to understand the problem (the structure of the PSI–PSII megacomplex) in accordance with known physical parameters (such as energy transfer speed).

Previous results showed that fast energy transfer occurs between PSII and PSI reaction centers (20 ps; Yokono et al. 2015). This result strongly suggests a direct connection between the core antennas of PSI and PSII in the PSI–PSII megacomplex, because energy transfer via a LHCII trimer bridge seems to be seven times slower (~150 ps; Caffarri et al. 2011). Thus, we decided on an initial guide model as shown in Supplementary Fig. S3B. Firstly, the outer contours of all particles were manually fitted to the initial guide model and particles that were successfully fitted were selected. If some additional structures were needed to fit the particles, these particles were excluded at this stage. Particles that could be assigned to other known complexes such as PSII megacomplexes (negative control models in Supplementary Fig. S3B) were also excluded; 5%, 6% and 2% of particles could be assigned to the PSII megacomplex, PSI megacomplex, and PSI–NDH complex, respectively. Then, the guide model was modified by adding new components such as LHCs and the same fitting procedures were repeated using particles excluded at the first fitting stage. These fitting processes were repeated if the number of successfully fitted particles increased by 10%. The final guide model fit 88% of particles. After the fitting process, we determined the frequencies of each component such as LHCs and PSI particles in the final model (Supplementary Fig. S3C). The fitting results are summarized in Supplementary Datasets.

Next, we superimposed all the images of successfully fitted particles (88% of the electron microscope images) and obtained averaged images of the PSI–PSII megacomplex (**Fig. 5A**). In this process, the orientations of the images of the particles were determined from the above fitting process on the basis of the rotational symmetry.

The size distribution of the megacomplexes from electron microscopy is shown in Supplementary Fig. S2A. Most of the large particles (>1,200 kDa) could contain both PSI and PSII. When the images of these particles were used for structural analysis, the guide model did not affect the physical arrangement of PSI and PSII in the megacomplex. A similar structure was obtained with the large particles (Supplementary Fig. S2B), indicating the present method was reliable.

Supplementary Data

Supplementary data are available at PCP online.

Funding

This work was supported by the Japan Science and Technology Agency [the CREST program (JPMJCR11B2) to A.T.] and the Japan Society for the Promotion of Science [KAKENHI grant 16H06553 to S.A.].

Acknowledgments

We are grateful to Dr. Motoshi Kunugi for providing algal thylakoids and Ms. Hiroko Uchida for treatment of macrophytic green algal samples. We thank Robbie Lewis, MSc, from Edanz Group (www.edanzediting.com/ac) for editing a draft of this manuscript.

Disclosures

M.Y. is an employee of Nippon Flour Mills Co., Ltd.

Author Contributions

M.Y. designed and performed the research. A.Takabayashi cultured unicellular green algae. A.M. collected and cultured macrophytic green algae. T.F. and M.I. prepared *P. patens* samples. A.Tanaka prepared purified standard samples. S.A. developed devices for time-resolved fluorescence measurement. M.Y. and A.Takabayashi arranged the CN-AGE system. J.K. developed procedures for grid preparation from CN-AGE gel strips, and performed electron microscopic measurements. M.Y. analyzed the data and wrote the paper. All authors reviewed and discussed the manuscript.

References

Albertsson, P.-Å. (2001) A quantitative model of the domain structure of the photosynthetic membrane. *Trends Plant Sci.* 6: 349–354.

Anderson, J.M. (2012) Lateral heterogeneity of plant thylakoid protein complexes: early reminiscences. *Philos. Trans. Royal Soc. B* 367: 3384–3388.

Andersson, B. and Anderson, J.M. (1980) Lateral heterogeneity in the distribution of chlorophyll-protein complexes of the thylakoid membranes of spinach chloroplasts. *Biochim. Biophys. Acta* 593: 427–440.

Ballottari, M., Alcocer, M.J., D'Andrea, C., Viola, D., Ahn, T.K., Petrozza, A., et al. (2014) Regulation of photosystem I light harvesting by zeaxanthin. *Proc. Nat. Acad. Sci. U.S.A.* 111: E2431–E2438.

Bell, A.J., Frankel, L.K. and Bricker, T.M. (2015) High yield non-detergent isolation of photosystem I-light-harvesting chlorophyll II membranes from spinach thylakoids, implications for the organization of the PS I antennae in higher plants. *J. Biol. Chem.* 290: 18429–18437.

Benson, S.L., Maheswaran, P., Ware, M.A., Hunter, C.N., Horton, P., Jansson, S., et al. (2015) An intact light harvesting complex I antenna system is required for complete state transitions in *Arabidopsis*. *Nat. Plants* 1: 15176.

Bos, I., Bland, K.M., Tian, L., Croce, R., Frankel, L.K., van Amerongen, H., et al. (2017) Multiple LHCII antennae can transfer energy efficiently to a single photosystem I. *Biochim. Biophys. Acta* 1858: 371–378.

Bressan, M., Bassi, R. and Dall'Osto, L. (2018) Loss of LHCI system affects LHCII re-distribution between thylakoid domains upon state transitions. *Photosynth. Res.* 135: 251–261.

Burke, J.J., Ditto, C.L. and Arntzen, C.J. (1978) Involvement of the light-harvesting complex in cation regulation of excitation energy distribution in chloroplasts. *Arch. Biochem. Biophys.* 187: 252–263.

Caffarri, S., Broess, K., Croce, R. and van Amerongen, H. (2011) Excitation energy transfer and trapping in higher plant photosystem II complexes with different antenna sizes. *Biophys. J.* 100: 2094–2103.

Caffarri, S., Kouřil, R., Kereïche, S., Boekema, E.J. and Croce, R. (2009) Functional architecture of higher plant photosystem II supercomplexes. *EMBO J.* 28: 3052–3063.

Chow, W., Ford, R. and Barber, J. (1981) Possible effects of the detachment of stromal lamellae from granal stacks on salt-induced changes in spillover. A study by sonication of chloroplasts. *Biochim. Biophys. Acta* 635: 317–326.

Correa-Galvis, V., Poschmann, G., Melzer, M., Stühler, K. and Jahns, P. (2016) PsbS interactions involved in the activation of energy dissipation in *Arabidopsis*. *Nat. Plants* 2: 15225.

Dinc, E., Tian, L., Roy, L.M., Roth, R., Goodenough, U. and Croce, R. (2016) LHCSR1 induces a fast and reversible pH-dependent fluorescence quenching in LHCII in *Chlamydomonas reinhardtii* cells. *Proc. Nat. Acad. Sci. U.S.A.* 113: 7673–7678.

Drop, B., Boekema, E.J. and Croce, R. (2014) Consequences of state transitions on the structural and functional organization of Photosystem I in the green alga *Chlamydomonas reinhardtii*. *Plant J.* 78: 181–191.

Falkowski, P.G., Katz, M.E., Knoll, A.H., Quigg, A., Raven, J.A., Schofield, O., et al. (2004) The evolution of modern eukaryotic phytoplankton. *Science* 305: 354–360.

Grieco, M., Suorsa, M., Jajoo, A., Tikkanen, M. and Aro, E.-M. (2015) Light-harvesting II antenna trimers connect energetically the entire photosynthetic machinery—including both photosystems II and I. *Biochim. Biophys. Acta* 1847: 607–619.

Henderson, G.P., Gan, L. and Jensen, G.J. (2007) 3-D ultrastructure of *O. tauri*: electron cryotomography of an entire eukaryotic cell. *PLoS One* 2: e749.

Hirashima, M., Satoh, S., Tanaka, R. and Tanaka, A. (2006) Pigment shuffling in antenna systems achieved by expressing prokaryotic chlorophyllide a oxygenase in *Arabidopsis*. *J. Biol. Chem.* 281: 15385–15393.

Holzwarth, A.R. (1996) Data analysis of time-resolved measurements. *In* Biophysical Techniques in Photosynthesis.Edited by Amesz, J. and Hoff, A.J. pp. 75–92. Springer, Dordrecht.

Horie, Y., Ito, H., Kusaba, M., Tanaka, R. and Tanaka, A. (2009) Participation of chlorophyll b reductase in the initial step of the degradation of light-harvesting chlorophyll *a*/*b*-protein complexes in *Arabidopsis*. *J. Biol. Chem.* 284: 17449–17456.

Järvi, S., Suorsa, M., Paakkarinen, V. and Aro, E.M. (2011) Optimized native gel systems for separation of thylakoid protein complexes: novel super- and mega-complexes. *Biochem. J.* 439: 207–214.

Kaňa, R. (2016) Role of ions in the regulation of light-harvesting. *Front. Plant Sci.* 7: 1849.

Kim, E., Akimoto, S., Tokutsu, R., Yokono, M. and Minagawa, J. (2017) Fluorescence lifetime analyses reveal how the high light–responsive protein LHCSR3 transforms PSII light-harvesting complexes into an energy-dissipative state. *J. Biol. Chem.* 292: 18951–18960.

Kirchhoff, H., Hinz, H.-J. and Roesgen, J. (2003) Aggregation and fluorescence quenching of chlorophyll a of the light-harvesting complex II from spinach in vitro. *Biochim. Biophys. Acta* 1606: 105–116.

Kouřil, R., Strouhal, O., Nosek, L., Lenobel, R., Chamrád, I., Boekema, E.J., et al. (2014) Structural characterization of a plant photosystem I and NAD (P) H dehydrogenase supercomplex. *Plant J.* 77: 568–576.

Kouril, R., Zygadlo, A., Arteni, A.A., de Wit, C.D., Dekker, J.P., Jensen, P.E., et al. (2005) Structural characterization of a complex of photosystem I and light-harvesting complex II of *Arabidopsis thaliana*. *Biochemistry* 44: 10935–10940.

Kunugi, M., Satoh, S., Ihara, K., Shibata, K., Yamagishi, Y., Kogame, K., et al. (2016) Evolution of green plants accompanied changes in light-harvesting systems. *Plant Cell Physiol.* 57: 1231–1243.

Kuwabara, T. and Murata, N. (1982) Inactivation of photosynthetic oxygen evolution and concomitant release of three polypeptides in the photosystem II particles of spinach chloroplasts. *Plant Cell Physiol.* 23: 533–539.

Leliaert, F., Verbruggen, H. and Zechman, F.W. (2011) Into the deep: new discoveries at the base of the green plant phylogeny. *Bioessays* 33: 683–692.

Liu, H., Zhang, H., Niedzwiedzki, D.M., Prado, M., He, G., Gross, M.L., et al. (2013) Phycobilisomes supply excitations to both photosystems in a megacomplex in cyanobacteria. *Science* 342: 1104–1107.

Masuda, T., Tanaka, A. and Melis, A. (2003) Chlorophyll antenna size adjustments by irradiance in *Dunaliella salina* involve coordinate regulation of chlorophyll *a* oxygenase (CAO) and *Lhcb* gene expression. *Plant Mol. Biol.* 51: 757–771.

Mazor, Y., Borovikova, A. and Nelson, N. (2015) The structure of plant photosystem I super-complex at 2.8 Å resolution. *Elife* 4: e07433.

Melis, A. (1975) Properties of photosystem II as determined by the kinetic analysis of chloroplast fluorescence. Ph.D. Thesis. Florida State University.

Melis, A. and Akoyunoglou, G. (1977) Development of the two heterogeneous photosystem II units in etiolated bean leaves. *Plant Physiol.* 59: 1156–1160.

Melis, A. and Homann, P.H. (1976) Heterogeneity of the photochemical centers in system II of chloroplasts. *Photochem. Photobiol.* 23: 343–350.

Melis, A. and Thielen, A. (1980) The relative absorption cross-sections of photosystem I and photosystem II in chloroplasts from three types of *Nicotiana tabacum*. *Biochim. Biophys. Acta* 589: 275.

Melkozernov, A.N., Kargul, J., Lin, S., Barber, J. and Blankenship, R.E. (2004) Energy coupling in the PSI-LHCI supercomplex from the green alga *Chlamydomonas reinhardtii*. *J. Phys. Chem. B* 108: 10547–10555.

Mimuro, M., Akimoto, S., Tomo, T., Yokono, M., Miyashita, H. and Tsuchiya, T. (2007) Delayed fluorescence observed in the nanosecond time region at 77 K originates directly from the photosystem II reaction center. *Biochim. Biophys. Acta* 1767: 327–334.

Morosinotto, T., Breton, J., Bassi, R. and Croce, R. (2003) The nature of a chlorophyll ligand in Lhca proteins determines the far red fluorescence emission typical of photosystem I. *J. Biol. Chem.* 278: 49223–49229.

Mullet, J.E., Burke, J.J. and Arntzen, C.J. (1980) Chlorophyll proteins of photosystem I. *Plant Physiol.* 65: 814–822.

Mussgnug, J.H., Wobbe, L., Elles, I., Claus, C., Hamilton, M., Fink, A., et al. (2005) NAB1 is an RNA binding protein involved in the light-regulated differential expression of the light-harvesting antenna of *Chlamydomonas reinhardtii*. *Plant Cell* 17: 3409–3421.

Niyogi, K.K. and Truong, T.B. (2013) Evolution of flexible non-photochemical quenching mechanisms that regulate light harvesting in oxygenic photosynthesis. *Curr. Opin. Plant Biol.* 16: 307–314.

Rantala, M., Tikkanen, M. and Aro, E.M. (2017) Proteomic characterization of hierarchical megacomplex formation in *Arabidopsis* thylakoid membrane. *Plant J.* 92: 951–962.

Rochaix, J.-D. (2007) Role of thylakoid protein kinases in photosynthetic acclimation. *FEBS Lett.* 581: 2768–2775.

Ruban, A.V. (2016) Nonphotochemical chlorophyll fluorescence quenching: mechanism and effectiveness in protecting plants from photodamage. *Plant Physiol.* 170: 1903–1916.

Satoh, K., Strasser, R. and Butler, W. (1976) A demonstration of energy transfer from photosystem II to photosystem I in chloroplasts. *Biochim. Biophys. Acta* 440: 337–345.

Schaller, S., Richter, K., Wilhelm, C. and Goss, R. (2014) Influence of pH, Mg^{2+}, and lipid composition on the aggregation state of the diatom FCP in comparison to the LHCII of vascular plants. *Photosynth. Res.* 119: 305–317.

Schlodder, E., Hussels, M., Çetin, M., Karapetyan, N.V. and Brecht, M. (2011) Fluorescence of the various red antenna states in photosystem I complexes from cyanobacteria is affected differently by the redox state of P700. *Biochim. Biophys. Acta* 1807: 1423–1431.

Shubin, V.V., Bezsmertnaya, I.N. and Karapetyan, N.V. (1995) Efficient energy transfer from the long-wavelength antenna chlorophylls to P700 in photosystem I complexes from *Spirulina platensis*. *J. Photochem. Photobiol. B, Biol.* 30: 153–160.

Stewart, D.H., Cua, A., Bocian, D.F. and Brudvig, G.W. (1999) Selective raman scattering from the core chlorophylls in photosystem I via preresonant near-infrared excitation. *J. Phys. Chem. B* 103: 3758–3764.

Suorsa, M., Rantala, M., Danielsson, R., Järvi, S., Paakkarinen, V., Schröder, W.P., et al. (2014) Dark-adapted spinach thylakoid protein heterogeneity offers insights into the photosystem II repair cycle. *Biochim. Biophys. Acta* 1837: 1463–1471.

Sylak-Glassman, E.J., Malnoë, A., De Re, E., Brooks, M.D., Fischer, A.L., Niyogi, K.K., et al. (2014) Distinct roles of the photosystem II protein PsbS and zeaxanthin in the regulation of light harvesting in plants revealed by fluorescence lifetime snapshots. *Proc. Nat. Acad. Sci. U.S.A.* 111: 17498–17503.

Takabayashi, A., Niwata, A. and Tanaka, A. (2016) Direct interaction with ACR11 is necessary for post-transcriptional control of GLU1-encoded ferredoxin-dependent glutamate synthase in leaves. *Sci. Rep.* 6: 29668.

Takagi, D., Hashiguchi, M., Sejima, T., Makino, A. and Miyake, C. (2016) Photorespiration provides the chance of cyclic electron flow to operate for the redox-regulation of P700 in photosynthetic electron transport system of sunflower leaves. *Photosynth. Res.* 129: 279–290.

Takagi, D., Ishizaki, K., Hanawa, H., Mabuchi, T., Shimakawa, G., Yamamoto, H., et al. (2017) Diversity of strategies for escaping reactive oxygen species production within photosystem I among land plants: P700 oxidation system is prerequisite for alleviating photoinhibition in photosystem I. *Physiol. Plant.* 161: 56–74.

Tan, X.-X., Xu, D.-Q. and Shen, Y.-K. (1998) Both spillover and light absorption cross-section changes are involved in the regulation of excitation energy distribution between the two photosystems during state transitions in wheat leaf. *Photosynth. Res.* 56: 95–102.

Tanaka, A., Ito, H., Tanaka, R., Tanaka, N.K., Yoshida, K. and Okada, K. (1998) Chlorophyll a oxygenase (CAO) is involved in chlorophyll *b* formation from chlorophyll *a*. *Proc. Nat. Acad. Sci. U.S.A.* 95: 12719–12723.

Tiwari, A., Mamedov, F., Grieco, M., Suorsa, M., Jajoo, A., Styring, S., et al. (2016) Photodamage of iron–sulphur clusters in photosystem I induces non-photochemical energy dissipation. *Nat. Plants* 2: 16035.

Tokutsu, R., Kato, N., Bui, K.H., Ishikawa, T. and Minagawa, J. (2012) Revisiting the supramolecular organization of photosystem II in *Chlamydomonas reinhardtii*. *J. Biol. Chem.* 287: 31574–31581.

Tomo, T., Akimoto, S., Ito, H., Tsuchiya, T., Fukuya, M., Tanaka, A., et al. (2009) Replacement of chlorophyll with di-vinyl chlorophyll in the antenna and reaction center complexes of the cyanobacterium *Synechocystis* sp. PCC 6803: Characterization of spectral and photochemical properties. *Biochim. Biophys. Acta* 1787: 191–200.

Trissl, H.-W. (1997) Determination of the quenching efficiency of the oxidized primary donor of photosystem I, $P700^{+}$: implications for the trapping mechanism. *Photosynth. Res.* 54: 237–240.

Veerman, J., McConnell, M.D., Vasil'ev, S., Mamedov, F., Styring, S. and Bruce, D. (2007) Functional heterogeneity of photosystem II in domain specific regions of the thylakoid membrane of spinach (*Spinacia oleracea L.*). *Biochemistry* 46: 3443–3453.

Wientjes, E., Roest, G. and Croce, R. (2012) From red to blue to far-red in Lhca4: how does the protein modulate the spectral properties of the pigments? *Biochim. Biophys. Acta* 1817: 711–717.

Yadav, K.S., Semchonok, D.A., Nosek, L., Kouřil, R., Fucile, G., Boekema, E.J., et al. (2017) Supercomplexes of plant photosystem I with cytochrome b6f, light-harvesting complex II and NDH. *Biochim. Biophys. Acta* 1858: 12–20.

Yokono, M., Murakami, A. and Akimoto, S. (2011) Excitation energy transfer between photosystem II and photosystem I in red algae: larger amounts of phycobilisome enhance spillover. *Biochim. Biophys. Acta* 1807: 847–853.

Yokono, M., Takabayashi, A., Akimoto, S. and Tanaka, A. (2015) A megacomplex composed of both photosystem reaction centres in higher plants. *Nat. Commun.* 6: 6675.